INTERNATIONAL JOURNAL FOR NUMERICAL METHODS IN FLUIDS, VOL. 6, 459–477 (1986)

PERFORMANCE OF A MULTIGRID CALCULATION PROCEDURE IN THREE-DIMENSIONAL SUDDEN EXPANSION FLOWS

S. P. VANKA

Components Technology Division, Argonne National Laboratory, 9700 South Cass Avenue, Argonne, IL 60439, U.S.A.

SUMMARY

The performance of a recently developed calculation procedure for steady incompressible flows is assessed in a variety of three-dimensional sudden expansion type flows representative of those encountered in several types of industrial equipment. The calculation procedure, called here BLIMM (for *bl*ock-*im*plicit *m*ultigrid *m*ethod), is based on a coupled solution of the three-dimensional momentum and continuity equations in primitive variables, using the multigrid technique. Different Reynolds numbers and finite difference grids are considered for each flow situation. The rates of convergence and the computational times are reported for each case.

KEY WORDS Multigrids Laminar Flow Sudden Expansions

INTRODUCTION

In the last decade, computational fluid mechanics has occupied an important role in the design of many types of fluid flow equipment. In order to understand in detail the transport processes inside the flow passages, it is now becoming popular and beneficial to solve the governing partial differential equations numerically. A variety of flows which are steady or unsteady, laminar or turbulent, and incompressible or compressible have been considered in earlier studies.[1,2] For flows which are turbulent and/or reacting, physical models representing the macro behaviour of the processes are included in addition to the fluid flow equations. Such computational models have found application in various mechanical, aerospace, chemical, biological and environmental disciplines of fluid mechanics research.

One of the main goals of research in computational fluid dynamics is to provide reliable, accurate and economical solutions to the governing (partial differential) equations formulated to represent an industrial flow process. Decreases in computer time and storage requirements not only provide monetary benefits but also permit quick designs to be performed. Also, efficient solution of the equations means that a larger number of finite difference nodes that is usually necessary for establishing grid independency of the solution can be practically employed. However, despite many recent advances in computational fluid mechanics, accurate calculation of practical three-dimensional flows remains a difficult task. This is because in three dimensions the number of finite difference (or finite-element) nodes needed to represent the differential equations accurately can be as large as one or two million (say $100 \times 100 \times 100$). Such calculations require very large computer times and storage. Also, in many cases, the rate of convergence is inferior to that of an equivalent two-dimensional calculation. Because of the practical occurrence of three-dimensional flows, research in solving the relevant partial differential equations efficiently is of significant importance.

0271–2091/86/070459–19$09.50

Received 26 November 1985
Revised 21 January 1986

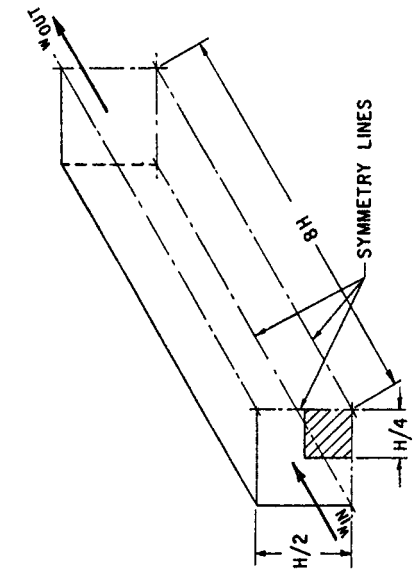

Figure 1(a). Laminar three-dimensional sudden expansion

Figure 1(b). Laminar three-dimensional blunt base flow

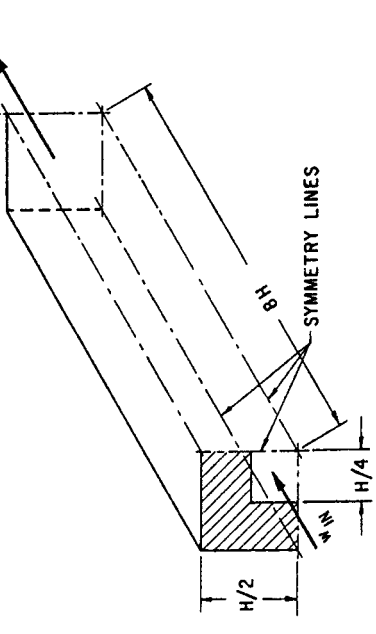

Figure 1(c). Model side-inlet combustor

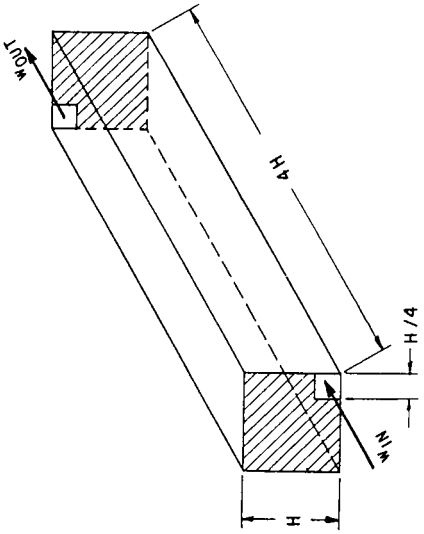

Figure 1(d). Rectangular box with diagonally opposite inlets

The present paper deals with the evaluation of a recently developed finite difference calculation procedure[3] for steady three-dimensional flows. The procedure solves the steady form of the Navier–Stokes equations in the primitive variable formulation in a coupled block-implicit manner using the multigrid technique.[4] The coupled (simultaneous) solution eliminates the need for the pressure or pressure correction equation by retaining the continuity equation in its primitive form in terms of velocities. Because of the coupling, the local mass continuity is implicitly satisfied during the calculation of the velocities. The use of the multigrid technique is advantageous on fine grids (commonly necessary for grid independent solution) because it maintains the same rate of convergence as on the coarser grids. Such a coupled multigrid solution was observed to be rapidly convergent in the calculation of the viscous flow in a driven cubic cavity.[3]

In this study, this earlier reported procedure is evaluated in a number of more complex flow situations representative of those encountered in industrial equipment. Four flow situations, sketched in Figure 1, are considered. They are:

(i) flow in a three-dimensional sudden expansion
(ii) flow over a blunt body
(iii) flow in a rectangular box
(iv) a model side-inlet combustor.

These situations represent, in a simplified way, several practical flows, such as those in furnaces, ramjet and gas turbine combustors, heat exchangers and the flame stabilization phenomena behind blunt bodies. For each flow situation two or three Reynolds numbers and two or three grids are considered. The rate of convergence of the algorithm is studied in detail. For the purpose of this study, all flows are considered to be laminar, incompressible and of uniform density.

SOLUTION PROCEDURE

The details of the currently used calculation procedure have been recently reported.[3] In this paper, therefore, only the important aspects of the procedure and its extension to general boundary conditions are described. The flows considered here are governed by the steady, laminar incompressible Navier–Stokes equations in their fully elliptic form. These equations in Cartesian co-ordinates are:

x-momentum

$$\partial(uu)/\partial x + \partial(vu)/\partial y + \partial(wu)/\partial z = -\partial p/\rho\partial x + \nu(\partial^2 u/\partial x^2 + \partial^2 u/\partial y^2 + \partial^2 u/\partial z^2), \tag{1}$$

y-momentum

$$\partial(uv)/\partial x + \partial(vv)/\partial y + \partial(wv)/\partial z = -\partial p/\rho\partial y + \nu(\partial^2 v/\partial x^2 + \partial^2 v/\partial y^2 + \partial^2 v/\partial z^2), \tag{2}$$

z-momentum

$$\partial(uw)/\partial x + \partial(vw)/\partial y + \partial(ww)/\partial z = -\partial p/\rho\partial z + \nu(\partial^2 w/\partial x^2 + \partial^2 w/\partial y^2 + \partial^2 w/\partial z^2), \tag{3}$$

Mass continuity

$$\partial u/\partial x + \partial v/\partial y + \partial w/\partial z = 0. \tag{4}$$

The boundary conditions for these equations are different for each flow situation and consist of both Dirichlet (fixed values) and Neuman conditions. At the outflow boundaries, extrapolative conditions (with zero derivatives) are used. The finite difference forms of the above differential equations are derived by integrating them over discrete control volumes in the flow domain. A staggered mesh system is used in which the discrete velocities are located on the faces of the finite difference cells and the discrete pressures are situated at the cell centres. The hybrid differencing scheme[5] is used to finite difference the differential expressions. In this well-known scheme, both first and second derivatives are initially written in terms of central differences. However, for stability reasons, in regions where the cell Reynolds number is greater than two, the convective term in the corresponding flow direction is expressed by an 'upwind' formulation and the diffusional flux is made zero. This practice ensures that the finite difference equation remains stable and correctly depicts the variation of the interface value with the local Reynolds number. Although the hybrid differencing is only first-order accurate at high Reynolds numbers and thus is diffusive, it has been used in a number of earlier studies because currently it offers the best compromise between accuracy and stability. Other alternative schemes[6,7] offer formally better accuracy; however, so far the experience has been that they slow down the rate of convergence significantly and generate over- and undershoots in the transport variables.[8]

The finite difference equations, expressed per unit volume (for convenience in the use of the multigrid technique), can be written in the general form

$$A_P\phi_P = \sum_i A_i\phi_i + S^\phi, \tag{5}$$

where ϕ stands for u, v or w, and S is the pressure gradient term in the appropriate direction. The summation is over all the neighbour values of point P in the x^+, x^-, y^+, y^-, z^+ and z^- directions. The coefficients A_P and A_i represent the combined effects of convection and diffusion. Expressions for the coefficients are given in several earlier works and also in Reference 3.

The continuity equation is differenced in its primitive form in terms of velocities. Thus, it is written as

$$(u_{x^+} - u_{x^-})/\delta x + (v_{y^+} - v_{y^-})/\delta y + (w_{z^+} - w_{z^-})/\delta z = 0, \tag{6}$$

where the + and − subscripts refer to the sides of a cell surrounding a finite difference node. δx, δy and δz represent the mesh sizes in the three directions.

The current solution algorithm, BLIMM, differs in two major aspects from several others earlier reported in the literature for internal flows (e.g. SIMPLE, SIMPLER,[1] CELS[9]). The two salient features in the present algorithm are the use of the multigrid technique of Brandt[4] and the coupled relaxation of the momentum and continuity equations without deriving an equation for pressure or pressure correction. In relation to the works of Fuchs and Zhao[10] who employ Brandt's[4] distributive Gauss–Seidel technique, the present relaxation operator implicitly retains the pressure–velocity coupling between the momentum and continuity equations. Such a relaxation operator is followed on the basis of several recent experiences[11–14] that the precise treatment of pressure–velocity coupling plays an important role in the rate of convergence, at least in viscous internal flows.

The concept of using multiple grids is well known.[4] Basically, any unconverged solution to a set of discrete elliptic equations contains errors of a wide range of frequencies. Traditional single grid iterative schemes such as Gauss–Seidel, ADI, etc. are efficient in annihilating errors of wavelengths comparable to the mesh size, but their convergence for low frequency errors is quite slow. However, frequencies small on one grid are relatively large on a coarser grid. Thus, cycling between the fine grid and a series of coarse grids can annihilate errors of all frequencies in an optimal way.

Several variants of multigrid cycling are possible. The present technique uses the full-

approximation-storage–full-multigrid (FAS–FMG) cycle suitable for non-linear problems. An adaptive strategy is used for switching between grids. Briefly, the procedure is as follows. After the finest grid is prescribed, a series of coarse grids is generated by successively doubling the mesh size in all three directions. The solution is then started on the coarsest grid. For this grid, the solution to the complete non-linear problem is sought to a prescribed accuracy. This solution is then 'prolongated' (extrapolated) to the next finer grid. Iterations are then made on this second grid until the high frequency errors are smoothed out. At this stage, the solution and the residuals in the equations are restricted to the coarser grid and the non-linear problem is solved with the residuals added to the right hand side. The modified coarse grid equation is

$$\mathbf{L}^1\mathbf{q}^1 = \mathbf{F}^1 + \mathbf{I}_2^1(\mathbf{F}^2 - \mathbf{L}^2\mathbf{q}^2), \tag{7}$$

where $\mathbf{L}^1$ and $\mathbf{L}^2$ are the non-linear operators on grids 1 and 2. $\mathbf{I}_2^1$ is the restriction operator for interpolating grid 2 values to grid 1. The second term on the right hand side is the restricted residual of grid 2. Equation (7) is then solved to a prescribed accuracy, after which the result is used to correct the solution on grid 2. The grid 2 values are corrected by adding to them the difference between the solution of equation (7) and the originally restricted grid 2 values. Thus

$$\mathbf{q}_{\text{new}}^2 = \mathbf{q}_{\text{old}}^2 + \mathbf{I}_1^2(\mathbf{q}_1 - \mathbf{I}_2^1\mathbf{q}_{\text{old}}^2), \tag{8}$$

where $\mathbf{q}^1$ and $\mathbf{q}^2$ represent the solution vectors on grids 1 and 2. $\mathbf{I}_1^2$ is the prolongation operator to extrapolate values from grid 1 to grid 2. Note that in this correction phase, only the *change* and not the solution ($\mathbf{q}^1$) is prolongated.

The corrected solution from equation (8) is then further iterated until the high frequency errors are again smoothed. The remaining residuals are again restricted to grid 1 and annihilated. The restrictions and prolongations are so continued until the solution on grid 2 is obtained to a desired prespecified accuracy. The solution on grid 2 is then used to obtain the first estimate of the solution on grid 3. After the high frequency errors on grid 3 are removed, the residuals are restricted to grid 2 and smoothed on grids 2 and 1. The solution on grid 3 is obtained by cycling between grids 3, 2 and 1. Progressively finer and finer grids are considered in sequence until the solution on the finest grid is obtained.

Relaxation procedure

The finite difference equations on any grid are solved simultaneously by a point Gauss–Seidel procedure. At each node, the momentum equations corresponding to the velocities on all the six faces of the cell and the continuity equation are solved in a coupled manner. The equations are linearized about the existing values (i.e. the A coefficients in equation (5) are evaluated from velocities in computer store), and a set of seven linear equations for the corrections is solved by inverting a bordered matrix. This symmetrical coupled Gauss–Seidel (SCGS) scheme is found to have a faster convergence rate *vis-à-vis* an unsymmetrical coupled operator in which only three velocities corresponding to the minus or plus side faces are solved along with the continuity equation. The solution of all the six velocities of any given cell is not any more expensive than the solution of only three velocities because the central coefficients are stored and reused. In order to maintain numerical stability, the central coefficients are divided by an under-relaxation factor α. Complete details of the present solution algorithm are given by Vanka.[3]

Restriction and prolongation

Restriction refers to the process of evaluating coarse grid residuals and solution from fine grid values. Prolongation is the opposite process of obtaining fine grid values and corrections from

coarse grid solution. In a full coarsening strategy, the coarse grid is obtained by doubling the mesh size of the next finer grid in all the three directions. Thus the number of finite difference cells is decreased by a factor of eight. Because of the use of a staggered mesh arrangement, different relations are necessary for each of the three velocity components and the pressure. To obtain a coarse grid velocity four fine grid values are averaged. For the pressure eight nearby fine grid pressures are averaged with equal weights. The relations are quite straightforward and can be found in Reference 3. For extrapolating the solution as well as the changes from the coarse grid to the next finer grid, a trilinear relation is used. Eight fine grid values are derived from eight surrounding coarse grid values by assuming a linear variation along each direction. These relations are also given in Reference 3.

An alternative to full coarsening is semi or S-coarsening.[4] S-coarsening is advantageous in flows where the streamlines are strongly aligned with one of the co-ordinate directions. In such flows, point relaxation schemes such as the one used here can be slow in convergence. Therefore line or plane relaxation schemes may be necessary for rapid smoothing of the high frequency components. However line or plane relaxation schemes are expensive because they involve some form of Gaussian elimination. As an alternative to line and plane relaxation, semi-coarsening can be employed. In semi-coarsening, the grid is coarsened only in the two directions normal to the predominant flow direction. Thus the grid spacing in the predominant flow direction is retained as that of the finest grid. The number of cells in a coarse grid is only a quarter (rather than an eighth) of the number in the next finer grid. Therefore, the CPU time and storage for the coarse grid iterations are larger for semi-coarsening than for full coarsening. However, this can be compensated for by a reduction in the number of fine grid iterations, owing to better asymptotic convergence.

The relations for restriction and prolongation for semi-coarsening are similar to those for a two-dimensional calculation. Thus, two fine grid values (in the plane of coarsening) are averaged to obtain one coarse grid velocity or a coarse grid residual in the momentum equations. For pressure and continuity residuals four (instead of eight) fine grid values are averaged. In prolongation, four pressures (or changes) of a coarse grid give four fine grid values, and two coarse grid velocities (or changes) give correspondingly prolongated fine grid velocities.

The flow situations considered in this study are highly complex flows, containing mixed regions of streamline alignment and flow recirculation. For example, in the sudden expansion flow of Figure 1(a), the inlet jet is aligned with the grid in the central region, but the top wall and corner regions contain the recirculating eddy. In the downstream region after reattachment, the streamlines are all one way, but the flow is more diffused owing to the expansion of the jet. In such a situation, precise *a priori* determination of the correct strategy is difficult. Other situations shown in Figure 1 are even more complex than the sudden expansion flow. Therefore in this study, calculations have been made with both full and semi-coarsening to evaluate their relative performance. In addition, corrections to satisfy integral mass balances across xy planes are made to enhance convergence.

Extension to non-Dirichlet boundary conditions

Some of the flow situations considered in this study involve non-Dirichlet boundary conditions. At the symmetry planes, the normal velocity is zero and other variables have zero normal derivatives. When Dirichlet conditions are not prescribed at the outflow boundary, a zero derivative extrapolative condition is used. Consequently, the normal velocity (located on the forward face of the cell) is taken to be that at the backward face of the cell and the other two velocities and the near-boundary pressure are calculated by solving the momentum and continuity equations for the near-boundary plane.

The incorporation of non-Dirichlet conditions requires some care to prevent slowing down of

the convergence in comparison with an equivalent Dirichlet boundary condition. At an outflow boundary, because of the one-way flow, the main linkage with the outflow velocities comes only in the continuity equation (note: diffusion is cut off due to hybrid differencing). Therefore only the treatment of the continuity equation is important. In this regard, it is necessary to satisfy two requirements. First, the outflow velocities on all grids must satisfy the overall mass continuity. This means that on all grids the condition

$$\oint \mathbf{V}\cdot\mathbf{n}\,ds = 0 \tag{9}$$

must be satisfied. Failure to satisfy this requirement will result in slow convergence or no convergence at all. In flows with density variations, the condition

$$\oint \rho\mathbf{V}\cdot\mathbf{n}\,ds = 0 \tag{10}$$

must be satisfied.

The second feature of the extrapolative outflow condition is during the restriction stage from fine to coarse grids. When a coarse grid is reached through restriction from a finer grid, it is necessary to remember that the equations actually solved are different from the original flow equations because of the additional restricted residuals. Thus, the total outflow from the boundary is not necessarily equal to the inflow. If the outflow velocities are modified as usual, then the implied outflow will be inconsistent and will lead to non-convergence. Therefore, when a coarse grid is reached as a restriction grid, the extrapolative boundary conditions must not be imposed. Instead, the coarse grid equations should be solved with restricted boundary velocities as Dirichlet conditions. When all coarse grids during restriction are completed, and final corrections to the local fine grid are made, the extrapolative conditions must be imposed. Such a practice is followed also for symmetry planes where zero normal flow and zero normal derivatives are enforced.

It is necessary to point out that it is very essential to ensure that the fine and coarse grids are consistent between themselves. Any error usually results in non-convergence with repeated switching between a fine and a coarse grid. Therefore, care must be exercised in programming the restriction and prolongation operators and the updating of the boundary conditions. Another point of importance is the level of the pressure field. In incompressible flows, the pressure is determined up to an additive constant, i.e. the level is arbitrary. Therefore, it is necessary to subtract the pressure at a reference point from the calculated pressures in order to keep the level from becoming arbitrarily large.

TEST CALCULATIONS

The main purpose of this study has been to assess the rate of convergence of the earlier reported calculation procedure[3] in more-complex three-dimensional flows representing commonly encountered industrial flows. Therefore, the algorithm is first extended to handle non-Dirichlet conditions, and is ensured to converge at nearly the same rate as with Dirichlet conditions. Also, the algorithm is programmed into a more general computer program that can handle several flows through changes only in the input data. This is achieved by allowing each boundary to consist of an arbitrary number of segments with each segment having the flexibility of a different boundary condition (inflow, outflow, symmetry line and wall).

In this study, four flow situations are considered. Each situation differs considerably from the others through unique flow field development and flow complexity. Each flow offers varying degrees of combination of zones of predominant flow with zones of flow recirculation. Therefore,

the calculations currently performed are stringent tests of the ability of the algorithm to calculate practical fluid flows.

For each geometrical configuration, two or three Reynolds numbers and two or three finite difference grids are considered. All calculations are started from plug distributions of axial velocity and null values for cross-stream velocities and pressure. Sensitivity tests are performed to determine the optimum under-relaxation factor. The calculations are made with full as well as semi-coarsening and the rate of convergence and the required CPU times on an IBM 3033 FORTHX compiler are tabulated for each test calculation. Some plots of the convergence history are given in Figures 2–10. Because the emphasis in this study has been on the rate of convergence, no efforts have been made to compare the flow fields with any existing data (in fact, because of the idealization of some of the geometries, no such experimental data may exist). However, the flow fields are checked for plausibility and qualitative correctness.

For the flow in a three-dimensional expansion, a 4:1 area ratio is considered. A total duct length of eight duct heights is considered. Because of symmetry conditions, only a quarter section of the duct with two symmetry planes is calculated. The finest mesh used contains more than 16,000 nodes with $16 \times 16 \times 64$ cells in the x, y and z directions, respectively. Three values of the flow Reynolds number (defined as $w_{in}H/\nu$) of 200, 400 and 800 are considered. Because of the large expansion ratio, the recirculation zone in these calculations is quite long. Consequently it has been necessary to use cells of large aspect ratio. Figures 2 and 3 show the rate of convergence for Reynolds numbers of 400 and 800 with full and semi-coarsening. The quantity plotted is an average of the residuals in the four equations, defined as

$$|R| = [\sum\{(R^u)^2 + (R^v)^2 + (R^w)^2 + (R^C)^2\}/(\mathrm{NEQ})]^{1/2}, \tag{11}$$

where NEQ = IMAX × JMAX × KMAX × 4 and the summation is made over all cells. R^u, R^v, R^w and R^C are point residuals (per unit cell volume) in the appropriate equations normalized by inlet momentum and inlet mass as appropriate. This norm of residuals is converged to a level less than 10^{-3} which is observed to provide a solution of good accuracy. The optimal values of the under-relaxation factor, the numbers of fine grid iterations, the equivalent work units, the CPU times

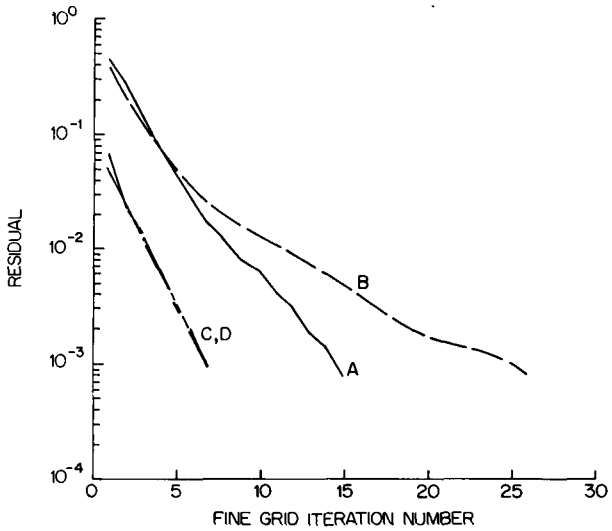

Figure 2. Rate of convergence for flow in a three-dimensional expansion, $Re = 400$: (A) $8 \times 8 \times 32$, full coarsening; (B) $16 \times 16 \times 64$, full coarsening; (C) $8 \times 8 \times 32$, semi coarsening; (D) $16 \times 16 \times 64$, semi coarsening.

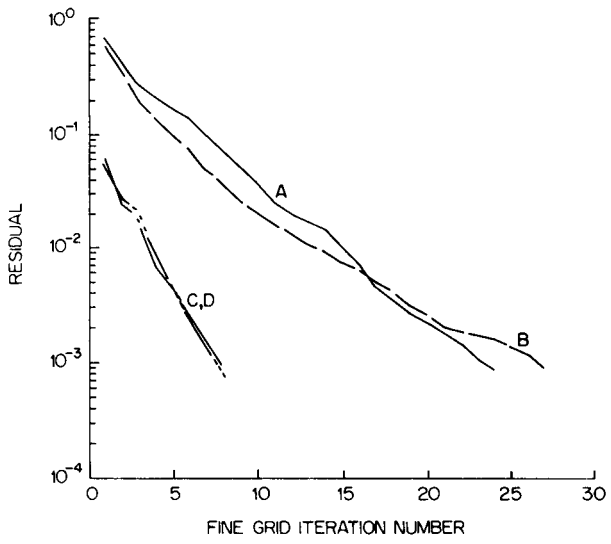

Figure 3. Rate of convergence for flow in a three dimensional expansion, $Re = 800$

and the smoothing factors for these calculations are tabulated in Tables I and II. The smoothing factor is defined as the rate of reduction of the residual per work unit. A work unit is time required for one fine grid iteration.

From Figures 2 and 3 and Tables I and II, the following conclusions can be drawn. First, the algorithm is rapidly convergent with no under-relaxation (except at $Re = 900$ with full coarsening). Typically, convergence is obtained in 15–30 fine grid iterations. Secondly, for this problem, semi-coarsening is seen to be advantageous over full coarsening. With semi-coarsening, convergence is obtained typically in 10 fine grid iterations (a total of 20 work units). The CPU times

Table I. Convergence details with full coarsening for laminar sudden expansion flow, $Z = 8{\cdot}0$

Grid	Item*	Re 200	Re 400	Re 800
8 × 8 × 32	A	1·0	1·0	0·8
	B	16	15	24
	C	23	22	36
	D	14·0	13·3	21·3
	E	0·80	0·75	0·83
16 × 16 × 64	A	1·0	1·0	0·8
	B	30	26	27
	C	45	39	43
	D	225·0	205·0	217·0
	E	0·88	0·85	0·86
Exponent		1·33	1·31	1·11

* A = Optimal under-relaxation factor
B = Number of fine grid iterations
C = Number of work units
D = CPU time, s
E = Smoothing factor

Table II. Convergence details with semi-coarsening for laminar sudden expansion flow, $Z = 8.0$

Grid	Item*	Re 200	Re 400	Re 800
8 × 8 × 32	A	1·0	1·0	1·0
	B	8	7	8
	C	14	13	17
	D	8·76	8·02	10·54
	E	0·72	0·73	0·78
16 × 16 × 64	A	1·0	1·0	1·0
	B	10	7	8
	C	18	14	20
	D	94·0	72·0	98·0
	E	0·77	0·73	0·81
Exponent		1·14	1·05	1·07

*See legend on Table I.

are observed to vary nearly linearly. The exponent is found to be close to unity for semi-coarsening but somewhat larger with full coarsening (note: exact linearity with semi-coarsening is possible by some 'fine-tuning' in the termination and switching criteria).

Figures 4–7 present the rate of convergence for the flow over a blunt body. This flow is geometrically inverse of the three-dimensional sudden expansion. In this case, the recirculation zone is established behind the blunt body instead of at the top wall. Two duct lengths of four and eight duct heights are considered and calculations for only one quarter of the duct cross-section are made. Three Reynolds numbers ($w_{in}H/\nu$) of 400, 800 and 1600 are considered for each case with the finest grid containing 16 × 16 × 64 cells (three levels with 8 × 8 × 32 and 4 × 4 × 16 cells).

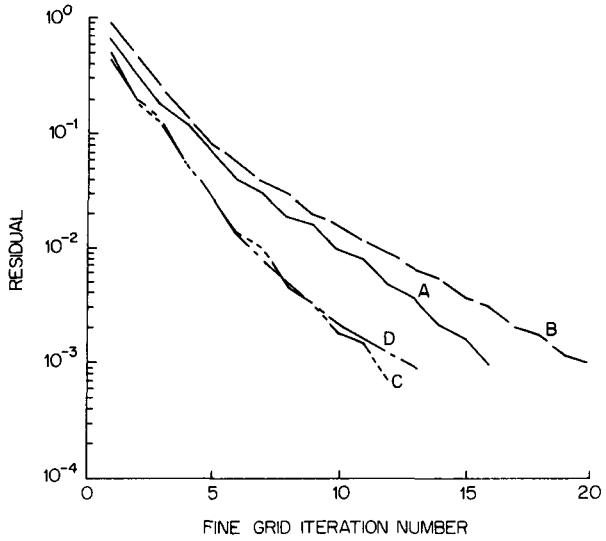

Figure 4. Rate of convergence for blunt base flow, $Re = 400$, $Z = 4{\cdot}0$

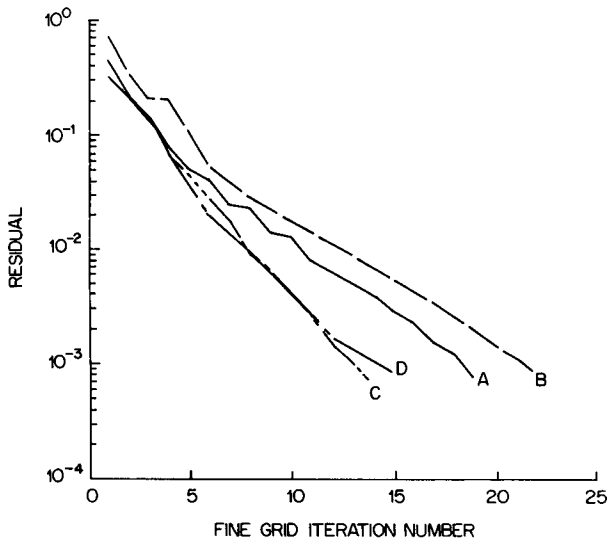

Figure 5. Rate of convergence for blunt base flow, $Re = 800$, $Z = 4{\cdot}0$

Calculations with both full and semi-coarsening have been made. The results of these calculations are tabulated in Tables III–VI. These timings and rates of convergence correspond to an accuracy level of 10^{-3} in the residual, as before.

For the blunt body calculations with a length of four duct heights, it is seen that both full and semi-coarsening converge at nearly the same rate. The exponent of work increase between fine and coarse grids to close to unity, as expected. However, when the duct length is increased to eight duct heights (with the aspect ratio of cells equal to four), the full-coarsening strategy is inferior to semi-coarsening. Typically, a factor of two improvement in CPU time is observed

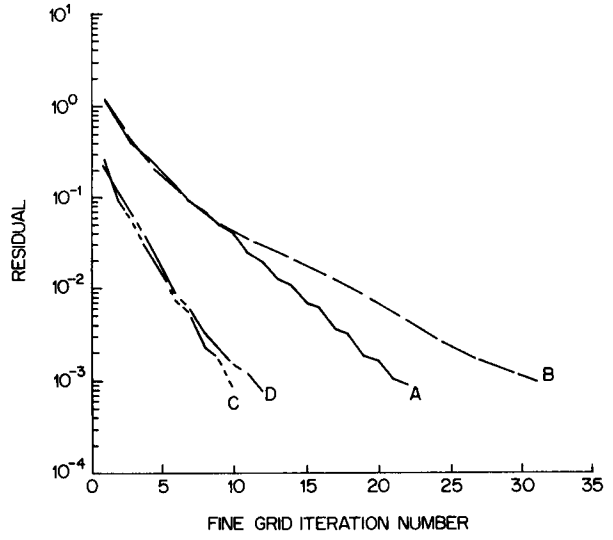

Figure 6. Rate of convergence for blunt base flow, $Re = 400$, $Z = 8{\cdot}0$

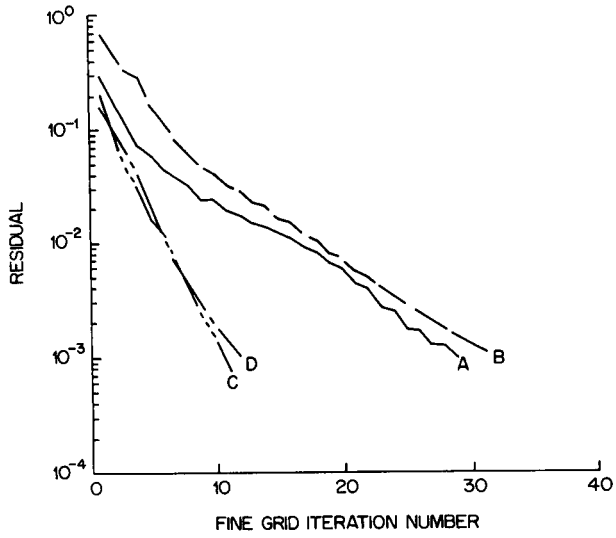

Figure 7. Rate of convergence for blunt base flow, $Re = 800$, $Z = 8{\cdot}0$

with semi-coarsening. Nevertheless the CPU times with both full and semi-coarsening are quite small.

The third flow situation considered is a rectangular representation of a side-inlet dump combustor of a liquid-fuelled ramjet.[15,16] In this geometry, the flow enters a rectangular duct from the top at an angle, as shown in Figure 1(c). The angled injection sets up a recirculation region behind the inlet jet, a stagnation region at the point of impingement and a top wall recirculation region. In the downstream section, the flow is nearly one-way after the reattachment region. This problem is a three-dimensional version of the geometry recently calculated by Vanka.[17]

For this geometry, the Reynolds number is defined to be $v_{in}Z/\nu$. A total length of six duct heights is considered. Only half of the cross-section is calculated because normally there are two

Table III. Convergence details with full coarsening for laminar blunt base flow, $Z = 4{\cdot}0$

Grid	Item*	Re 400	Re 800	Re 1600
8 × 8 × 32	A	0·9	0·9	0·7
	B	16	19	20
	C	24	29	30
	D	14·4	17·6	18·0
	E	0·76	0·80	0·82
16 × 16 × 64	A	0·9	0·9	0·7
	B	20	22	25
	C	31	35	41
	D	158·0	181·0	207·0
	E	0·80	0·82	0·85
Exponent		1·151	1·120	1·174

* See legend on Table I.

Table IV. Convergence details with full coarsening for laminar blunt base flow, $Z = 8{\cdot}0$

Grid	Item*	Re 400	Re 800	Re 1600
8 × 8 × 32	A	0·8	0·8	0·8
	B	22	25	29
	C	32	37	43
	D	19·3	22·0	26·2
	E	0·79	0·83	0·87
16 × 16 × 64	A	0·8	0·8	0·8
	B	31	29	32
	C	49	49	55
	D	258·0	254·0	278·0
	E	0·86	0·86	0·88
Exponent		1·246	1·176	1·136

*See legend on Table I.

inlet ports which are located symmetrically. Calculations are made for three values of the Reynolds number of 600, 1200 and 2400 and two grids containing 8 × 8 × 32 and 16 × 16 × 64 finite difference cells. The corresponding aspect ratios of the cells are 1·5 and 3·0 in the xz and yz planes, respectively. For this geometry also, both full and semi-coarsening are investigated. The calculations are initiated with plug axial velocity and null secondary velocity and pressure distributions. The calculation is terminated when the residual norm is below 10^{-3}. The rates of convergence for two of the three Reynolds numbers are shown in Figures 8 and 9. It is seen that convergence is obtained typically in 25 fine grid iterations for all the three Reynolds numbers. For this case, full coarsening is seen to be superior to semi-coarsening. The CPU times, optimal relaxation factors, average decreases in residuals per work unit and the numbers of fine grid iterations are given in Tables VII and VIII.

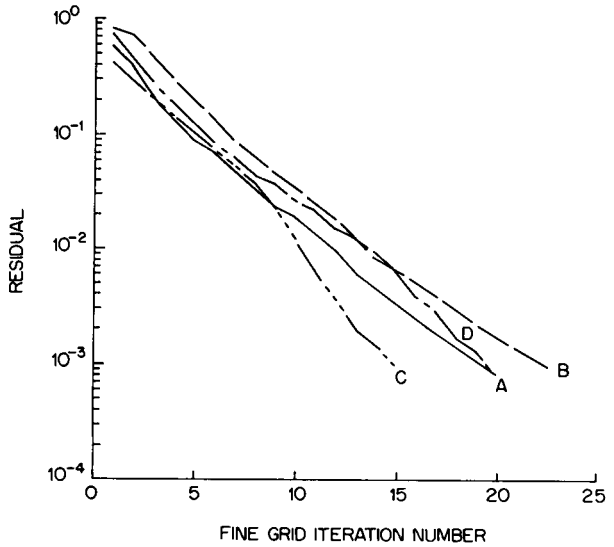

Figure 8. Rate of convergence for model side-inlet combustor, $Re = 600$

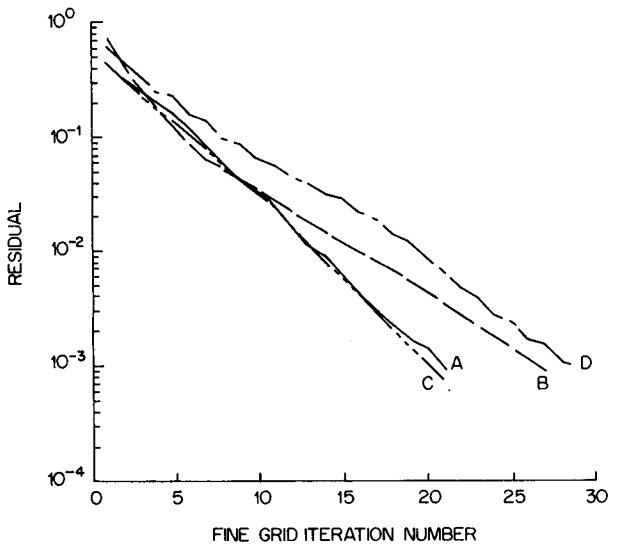

Figure 9. Rate of convergence for model side-inlet combustor, $Re = 2400$

The fourth situation calculated is the complex flow field established in a rectangular box when flow enters from one of the corners and exits from an opposite corner (shown in Figure 1(d)). The geometry is a model of the flow fields in nuclear reactor (breeder) plena, heat exchangers and ventilation flow in buildings. For this situation, the length of the box is taken equal to four duct heights. Three Reynolds numbers ($w_{in}H/\nu$) equal to 200, 400 and 800 are calculated with grids containing $8 \times 8 \times 16$ and $16 \times 16 \times 32$ cells. For this geometry only full coarsening is calculated because there is no predominant one-way flow, and initial calculations with semi-coarsening displayed slow convergence. The results for this case are tabulated in Table IX. It is seen that convergence is rapid, although some improvement is desirable. The appropriate smoothing factors are given in Table IX. Figure 10 shows the rate of convergence for the intermediate Reynolds number of 400.

Table V. Convergence details with semi-coarsening for laminar blunt base flow, $Z = 4{\cdot}0$

Grid	Item*	*Re* 400	800	1600
$8 \times 8 \times 32$	A	1·0	1·0	1·0
	B	16	14	12
	C	34	30	24
	D	21·1	18·7	14·8
	E	0·82	0·80	0·76
$16 \times 16 \times 64$	A	1·0	1·0	0·9
	B	13	15	16
	C	31	37	40
	D	162·0	191·0	208·0
	E	0·81	0·84	0·85
Exponent		0·980	1·117	1·27

*See legend on Table I.

Table VI. Convergence details with semi-coarsening for laminar blunt base flow, $Z = 8{\cdot}0$

Grid	Item*	*Re* 400	800	1600
8 × 8 × 32	A	1·0	1·0	0·9
	B	10	10	11
	C	18	19	23
	D	11·3	11·6	14·1
	E	0·73	0·74	0·79
16 × 16 × 64	A	1·0	1·0	0·9
	B	12	12	12
	C	26	26	28
	D	133·6	137·0	144·0
	E	0·80	0·79	0·82
Exponent		1·188	1·187	1·117

*See legend on Table I.

Table VII. Convergence details with full coarsening for model side-inlet combustor

Grid	Item*	*Re* 600	1200	2400
8 × 8 × 32	A	0·8	0·8	0·8
	B	20	21	21
	C	28	30	30
	D	16·7	17·3	17·8
	E	0·79	0·81	0·81
16 × 16 × 64	A	1·0	1·0	0·8
	B	23	24	27
	C	35	37	42
	D	174·0	184·0	214·0
	E	0·82	0·84	0·85
Exponent		1·127	1·136	1·195

*See legend on Table I.

CONCLUSIONS

In this study, we have extended an earlier reported calculation procedure to more complex boundary conditions and assessed its performance in four different flow situations of practical importance. For each flow situation, the Reynolds number, the finite difference grid and the numerical under-relaxation factor are varied. Finite difference grids containing up to 16,000 nodes have been considered. In all cases rapid convergence from initially guessed simplistic distributions has been obtained. The CPU times required for these calculations are much smaller than other widely used procedures, such as the SIMPLE[1] algorithm and its variants. Typically, an order of magnitude reduction in required CPU is observed based on earlier reported performance of the

Table VIII. Convergence details with semi-coarsening for model side-inlet combustor

Grid	Item*	Re 600	1200	2400
8 × 8 × 32	A	1·0	1·0	0·8
	B	15	18	21
	C	28	33	41
	D	16·7	19·7	24·2
	E	0·80	0·82	0·86
16 × 16 × 64	A	1·0	1·0	0·9
	B	20	23	29
	C	44	55	70
	D	221·0	272·0	348·0
	E	0·85	0·88	0·91
Exponent		1·242	1·262	1·282

*See legend on Table I.

Table IX. Convergence details with full coarsening for flow in a rectangular box, $Z = 4{\cdot}0$

Grid	Item*	Re 200	400	800
8 × 8 × 16	A	0·8	0·8	0·8
	B	14	15	21
	C	21	22	32
	D	5·50	6·12	8·61
	E	0·78	0·79	0·84
16 × 16 × 32	A	0·8	0·8	0·8
	B	18	20	22
	C	66·30	75·94	88·0
	D	27	31	37
	E	0·81	0·83	0·85
Exponent		1·19	1·20	1·11

*See legend on Table I

SIMPLE algorithm. This study demonstrates that the multigrid technique combined with a coupled relaxation of the equations shows promise for efficiently solving multidimensional fluid flows of practical relevance. The coupled relaxation of the equations is advantageous in situations where the pressure field plays an important role in flow redistribution. In comparison with the work involved for assembling the coefficients in the finite difference equations, the increase in work due to the coupled Gauss–Seidel operator is small. This time can be easily compensated for by the improved rate of convergence.

The present algorithm can be further improved in one or two ways. Currently, the FAS–FMG multigrid cycle is being used with an adaptive strategy. An adaptive strategy cycles through the grids in an automatic manner based on a rate of smoothing. Thus the procedure is more robust and

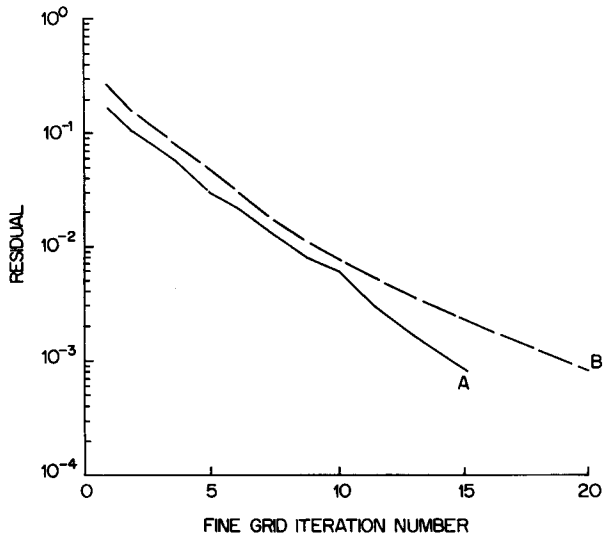

Figure 10. Rate of convergence for flow in a rectangular box, $Re = 400$: (A) $8 \times 8 \times 16$, full coarsening; (B) $16 \times 16 \times 32$, full coarsening

does not require user specifications such as that required in fixed-cycle algorithms. However, the adaptive cycling can result in some wastage of work when compared with an appropriate fixed-cycle strategy. It will be of interest to investigate the behaviour of a multigrid cycle based on a fixed strategy for the flow situations considered here. Secondly, the procedure can be combined with a marching procedure in regions where the flow is predominantly one way. This can be done by combining the multigrid procedure with the partially parabolic concept of Pratap and Spalding.[18] With such a capability, it will be possible to reduce the storage as well as the CPU time, thus permitting better concentration of grid cells in the fully elliptic regions. Such a procedure is currently under development.

The current exponents of the variation of CPU times are somewhat larger than the expected value of unity. This may have been due to some minor imperfections in the implementation of the multigrid technique as well as due to the problem complexity. Also, the solution is carried well beyond the truncation error limit into a region where the linearity of the multigrid technique is uncertain.[19] Currently a trilinear relation is used to prolongate both the solution and the changes from coarse to fine grids. Some improvement is also possible by using higher order prolongation operators for the solution.

In this study, finite difference grids containing up to 16,000 nodes have been considered. However, in Reference 3, calculations with a quarter of a million nodes ($64 \times 64 \times 64$) were made. Such calculations typically required 35 minutes on the IBM 3033 machine. The computer program used in the current study is more general than that of Reference 3. The current computer program is designed to solve six additional equations (four scalars and two turbulence variables) and contains provision for density and viscosity variations. Consequently, it requires three times more storage over the earlier simpler version. Because of this increase in storage, the next higher level of 128,000 nodes was not possible with the 8 megabyte core storage available on an IBM 3033. However, further fine grid calculations can be performed by using machines with larger storage, such as the CRAY X-MP/48.

Further work concerning the present algorithm is being focused on generalization of the

procedure to turbulent and reacting flows modelled through additional partial differential equations for scalar transport and turbulence variables. When this is completed, the procedure and the computer program can be used to study the multidimensional flow fields in industrial equipment such as furnaces, gas turbine combustors and liquid-fuelled ramjets.

ACKNOWLEDGEMENTS

This work was supported by the Ramjet Technology Division, Wright Patterson Air Force Base under an interagency agreement with Argonne National Laboratory. The author is grateful to Drs R. R. Craig and F. D. Stull for their support and encouragement.

NOMENCLATURE

A	Coefficient in the finite difference equation
ds	Elemental surface
F	Right hand side term in the finite difference equations
I	Restriction/prolongation operator
L	Finite difference operator
NEQ	Total number of finite difference equations
p	Pressure
q	Approximation to solution vector
$\|R\|$	Norm of residual in the finite difference equation
Re	Reynolds number
S	Source term in the finite difference equation
u, v, w	Velocity components in the x, y and z directions
V	Velocity vector
x, y, z	Co-ordinate directions
Z	Total length of flow domain
ρ	Density
ν	Kinematic viscosity
δ	Tolerance adjustment factor (= 0·2)
Subscripts	
i	Neighbour value
in	Inlet value
P	Central value
x, y, z	Values appropriate for x, y and z directions
new	New value
old	Old value
Superscripts	
C	Continuity equation
u, v, w	Values for u, v and w momentum equations

REFERENCES

1. S. V. Patankar, *Numerical Heat Transfer and Fluid Flow*, Hemisphere Publishing Corporation, 1980.
2. D. A. Anderson, J. C. Tannehill and R. H. Pletcher, *Computational Fluid Mechanics and Heat Transfer*, Hemisphere Publishing Corporation, 1984.
3. S. P. Vanka, 'A calculation procedure for three-dimensional recirculating flows', *Computer Methods in Applied Mechanics and Engineering*, to appear.
4. A. Brandt, 'Multigrid techniques: 1984 guide with applications to fluid dynamics', von Karman Institute, *Lecture Series 1984–04*, 1984.

5. D. B. Spalding, 'A novel finite-difference formulation for differential expressions involving both first and second derivatives', *Int. J. numer. methods eng.*, **4**, 551–559 (1972).
6. B. P. Leonard, 'A stable and accurate convective modeling procedure based on quadratic upstream interpolation', *Computer Methods in Applied Mechanics and Engineering*, **19**, 59–68 (1979).
7. G. D. Raithby, 'Skew upstream differencing for problems involving fluid flow', *Computer Methods in Applied Mechanics and Engineering*, **9**, 153–164 (1976).
8. S. P. Vanka, 'Study of second order upwind differencing in a recirculating flow', *NASA Contractor Report 174939*, June 1985.
9. P. F. Galpin, J. P. Van Doormal and G. D. Raithby, 'Solution of the incompressible mass and momentum equations by application of a coupled equation line solver', *Int. j. numer. methods fluids*, **5**, 615–625 (1985).
10. L. Fuchs and H. S. Zhao, 'Solution of three-dimensional viscous incompressible flows by a multigrid method', *Int. J. numer. methods fluids*, **4**, 539–555 (1984).
11. S. P. Vanka, 'Block-implicit calculation of steady turbulent recirculating flows', *International Journal of Heat and Mass Transfer*, **28**, 2093–2103 (1985).
12. S. P. Vanka, 'Calculation of axisymmetric turbulent confined diffusion flames', *AIAA Journal*, **24**, 462–469 (1986).
13. G. D. Raithby and G. E. Schneider, 'The numerical solution of problems in incompressible fluid flow: treatment of the velocity–pressure coupling', *Numerical Heat Transfer*, **2**, 417–440 (1979).
14. G. E. Schneider and M. Zedan, 'A coupled modified strongly implicit procedure for the numerical solution of coupled continuum problems', *AIAA-84-1743*, 1984.
15. F. D. Stull, R. R. Craig, G. D. Streby and S. P. Vanka, Investigation of a dual inlet side dump combustor using liquid fuel injection', *AIAA J. Propulsion and Power*, **1**, (1), 83–88 (1985).
16. S. P. Vanka, R. R. Craig and F. D. Stull, 'Mixing, chemical reaction and flow field development in ducted rockets', *AIAA J. Propulsion and Power*, to appear.
17. S. P. Vanka, 'Block-implicit multigrid calculation of two dimensional recirculating flows', *Computer Methods in Applied Mechanics and Engineering*, (to appear).
18. V. S. Pratap* and D. B. Spalding, 'Fluid flow and heat transfer in three-dimensional duct flows', *International Journal of Heat and Mass Transfer*, **19**, 1183–1188 (1976).
19. Tony F. Chan and Faisal Saied, 'A comparison of elliptic solvers for general two-dimensional regions', *Siam J. Sci. Stat. Comput.*, **6**, (3), (1985).

*Currently renamed as S. P. Vanka